Electron Microprobe Study of Otolith: Migratory Behavior and Habitat of Three Major Temperate Species of Eels

Yoshiyuki Iizuka

Institute of Earth Sciences, Academia Sinica

An analytical technique for measurement of strontium (Sr) and calcium (Ca) concentrations in otolith was developed using an electron probe micro-analyzer (EPMA). Precisions of measurement for Sr and Ca were examined with various electron beam conditions, which were a combination of different beam currents, beam diameter, X-ray counting time, and diffracting crystals on carbonate standards and eel otolith. The precision decreased when beam power densities exceeded 1 μW/μm^2 and/or beam diameter was less than 2 μm, resulting from beam damage of carbonates. The optimum analytical conditions for measuring the Sr/Ca ratios in the otoliths are suggested to be with a beam current at 3 nA, a 5 × 4 μm^2 beam, counting times of Sr and Ca for 80 sec and 20 sec at the peak, and of Sr and Ca for 20 sec and 10 sec at back-ground intensities at an acceleration voltage of 15 kV with strontianite and aragonite standards, respectively. In these conditions, it is possible to obtain precise measurements of Sr/Ca ratios at 10 μm intervals along a transect from the primordium (core) to the edge of individual otolith with an error less than 0.05 wt% in Sr, as these have been found to discriminate between brackish- and fresh-waters. We have studied more than 1,000 temperate eels from different water bodies where the East Asia (Japanese eels *Anguilla japonica*), the Northeast Ameria (American eels *Anguilla rostrata*), and the Northwest Europe (European Eel *Anguilla anguilla*). Patterns of otolith Sr/Ca ratios from core to edge indicated similar but multiple life histories, at least four to six type of migration behaviors. Additionally, the Sr/Ca patterns of otoliths clearly illustrate eels' life between naturally-recruited and artificially-restocked. Since Anguillid eels are the endangered species, the revealed habitat information from otolith microchemistry are variable and useful for conservation and cultivate studies.

Introduction

Otolith (ear-stone) of fish is an organ in the inner ear, which is composed of 3 types of otolith; sagitta, asteriscus, and lapillus, and functions for body balance and hearing. The otolith consists of approximately 95-6 wt% of calcium carbonate ($CaCO_3$), 3-4 wt% of organic matters, and less than 1 wt% of trace elements. The metabolically inert nature of the otolith assures that all mineralogical deposition remains unchanged throughout the life history of the fish [1]. Sagittal otolith is biomineralized aragonite which is deposited daily on a proteinaceous matrix [2, 3]. Aragonite has relatively higher substitution rate of the alkali earth elements, particularly Strontium (Sr), into the Ca site than the polymorphism calcite. In the seawater, Sr concentrations are approximately 100 fold higher than in freshwater environments. It is thought to be, therefore, that Sr can substitute for Ca in the process of otolith deposition during the seawater and brackish water residence [4]. Accordingly, temporal changes of the elements in sagittal otoliths can reflect the environment that a fish experienced. Ratios of Sr/Ca in otoliths were positively correlated to those in the ambient water [5]. Consequently, Sr/Ca ratios are extensively used to study the movement of diadromous fishes [e.g., 6-14]

Electron probe micro-analyzers (EPMA) equipped with wavelength dispersive X-ray spectrometers (WDS) have been widely used to determine chemical compositions of rock-forming minerals. The EPMA can analyze the calcium carbonate otolith at a limited area under observation of scanning electron micrograph. This is an advantage to target of analyses points on the otolith. It is well known, however, that carbonates are susceptible to damage from the electron beam. To avoid beam damage problem, consideration of electron beam setting and exposure time are essential in the development of high-precision analyses of otolith microchemistry [15-17].

The Sr/Ca ratios in otolith have been widely used for study of migratory history of fish since the late 1980s. Electron beam conditions and exposure times used for the quantitative analysis of Sr in otolith have greatly varied among laboratories. Gunn et al. [15] and Toole & Nielsen [17] indicated that the quantitative analysis of Sr in otoliths should be concern because of its low concentration. These researchers attempted to establish a criterion to analyze the Sr in otoliths by balancing the beam condition, in terms of beam power density (BPD)*, and beam exposure time to increase precision of the analyses of Ca and Sr. Gunn et

No.128, Sec. 2 Academia Road, Nankang Taipei, Taiwan 115, ROC

yiizuka@earth.sinica.edu.tw

al. [15] indicated that high BPD and long beam exposure time might cause pitting and induce a chemical change on the otolith. And then the BPD less than 3 μW/μm^2, which is maintained beam current at 25 nano ampere (nA) and beam diameter at 20 μm with an acceleration voltage of 15 kilo volt (kV), was recommended. The relative error of Sr contents in otoliths can be decreased by increasing the beam exposure time and lowering BPD. On the other hand, Toole & Nielsen [17] concluded that to increase analytical precision without losing accuracy, the BPD should be adjusted to approximately 15 μW/μm^2, i.e., maintaining beam current at 25 nA and beam diameter at 5 μm with an acceleration voltage of 15 kV. They also suggested that the behaviors of Sr and Ca are similar during beam damage, regardless of Ca concentration. However, this is not the case in the analysis of, at least, eel otoliths under their recommended conditions. By increasing beam exposure time, the intensity of Ca will increase and carbon (C) intensity will decrease (see below for further details). This may be due to a loss of material from the beam strike. Beam damage effects on the otolith surface and on target elements of the carbonates should be considered; otherwise it is difficult to evaluate small variations of Sr concentration (<1 wt%) in otoliths. In this paper, the author repots an examination of optimum technique of otolith study by EPMA and results of application studies of migratory history of eels.

Experimental procedure:

(1) Equipment

Elemental concentrations were quantified using an electron probe micro-analyzer (JEOL, JXA-8900R) at the Institute of Earth Sciences, Academia Sinica, Taipei, Taiwan. It is equipped with 4-channel WDS and programmed both qualitative (X-ray peak search, intensity counting and mapping) and quantitative (concentration) analyses. The quantitative data were corrected as oxides with standard calibration by the Phi-rho-z (PR-ZAF) method, which is a matrix correction with factors of atomic number (Z), absorption (A) and fluorescence (F) and depth distribution function (ρx), which represents the X-ray intensity per unit mass depth (ρz) [18, 19].

* Beam Power Density (μW/μm^2)=$[E_0 \times I]/A$, where E_0 is the acceleration voltage, I is the beam current and A is the area of electron beam on the surface of specimen.

(2) X-ray Diffracting crystals

For Ca $K\alpha$ measurement, the X-ray diffracting crystal Pentaerythritol (PETJ) was used. Two kind of diffracting crystals, PETH and Thallium Acid Phthalate (TAP) were used for measurement of Sr $L\alpha$. The diffracting crystals Lead Stearate (STE) was used for the measurement of C $K\alpha$. Each crystal is separately equipped in 3-different WDS channel of EPMA.

(3) Accelerating voltage

Acceleration voltage of 10-25 kV is generally used for rock-forming minerals. X-ray intensity from sample increases with accelerating voltage of the electron beam. However, the electron beam at higher voltage reaches deeper part of sample specimen and leads to decomposition of the specimen [20], and subsequently, X-ray intensity may alter during the analysis. Thus higher voltage (>20 kV) is typically applied to materials, which are damage-resistant to the electron beam, such as metal and metallic alloy. Lower voltage (<10 kV), on the other hand, is advantageous for light elements, though it is difficult to measure the X-ray intensity of the L-lines for such elements as Sr [19]. Therefore, the accelerating voltage was selected to be 15 kV, which is similar to some previous studies of otolith.

(4) Beam current

The beam current was tested from 1 to 20 nA. Minimum beam current was selected at 1 nA because a beam current lower than 1 nA was unable to detect the peak intensity of Sr in the otolith. Stabilities of the beam current were less than 0.25 % for 24 hr in all conditions.

(5) Otoliths and standard materials

Sagittal otolith of eel was extracted and mounted in

epoxy resin (EpoFix resin, Struers Co. Ltd) and then was ground and polished by aluminum compounds on polishing papers until the primordium was exposed. The otolith specimen was cleaned with distilled water in an ultrasonic bath and air dried before the carbon coating.

Chemical-known carbonates are selected for standard calibrations because of similar matrix compound to the otolith [21]. Calcite ($CaCO_3$ in the Trigonal system; NMNH 136321 [22]), a synthetic aragonite ($CaCO_3$, which is a polymorph of calcite, in the Orthorhombic system) and strontianite ($[Sr_{0.95}Ca_{0.05}]CO_3$ in Orthorhombic system [aragonite-structure]: NMNH R10065 [23]) were used as standards. The standards were mounted in epoxy resin and polished, then carbon-coated with the same thickness (approx. 25 nm [nano meter]) as the otolith specimens.

Establishment of Optimum beam condition

(1) Surface beam damage on otolith

Figure 1 shows damage spots on a polished otolith surface by various electron beams, BPD ranges from 0.1 to 376.8 μW/μm^2. The BPD is a combination of the beam current at 1–20 nA and a beam diameter of 1 (focused beam), 5 and 10 μm, and 5 × 4 μm^2 rectangle scanning beam, at the acceleration voltage of 15 kV for 100 seconds beam exposure. Surface observation under the secondary electron micrograph shows that higher BPD made stronger damage than lower BPD beam spot.

Relations between the X-ray intensities and beam exposure time were determined for Ca *Kα*, C *Kα* and Sr *Lα* of an otolith at the BPD ranging from 0.2 to 7.5 μW/μm^2, which are combinations of beam current between 3 nA and 10 nA, and beam size of 10 μm, 5 μm, 5 × 4 μm^2 (×20,000 in magnification) and 3 × 2 μm^2 (×30,000). The Ca, Sr and C intensities were counted for 5 sec × 50 cycles at the same spot after setting each peak position. Total beam exposure time is 250 sec at each analysis spot on the otolith surface.

The intensities of Ca, C and Sr were greater at higher than lower beam currents (**Fig. 2**a, b and c). At higher beam current, the intensities of Ca increased and C decreased with increasing exposure time, and the extent of alteration depended strongly upon the BPD. At a lower beam current, such as 3 nA and lower BPD (20k: 5 × 4 μm^2 rectangle beam), Ca intensities did not change throughout the analysis for 250 sec (Fig. 2a-1 and 2a-2), whereas the intensities of C were severely altered under the higher BPD beam compared with that of a larger beam size regardless of beam current (Fig. 2b). Changes in Sr intensities were smaller than those of other two elements regardless of the BPD and the exposure time (Fig. 2c). This indicates that the chemical composition of the otolith was changed by the beam strike with the electron current >10 nA or BPD >3.8 μW/μm^2, which is a beam of 5 nA and 5 μm in diameter. The otolith surface, as indicated by secondary electron images (Fig. 1), was also altered in the BPD is greater than 2 μW/μm^2, while pitting was reduced or not clearly observed at BPD <1 μW/μm^2. These indicate that chemical alteration occurred due to the material loss associated with pitted spots on the surface of otolith during beam exposure. Accordingly, the otolith surface was undoubtedly damaged by high BPD and high beam current. The extent of damage depends upon the magnitude of BPD and beam exposure time.

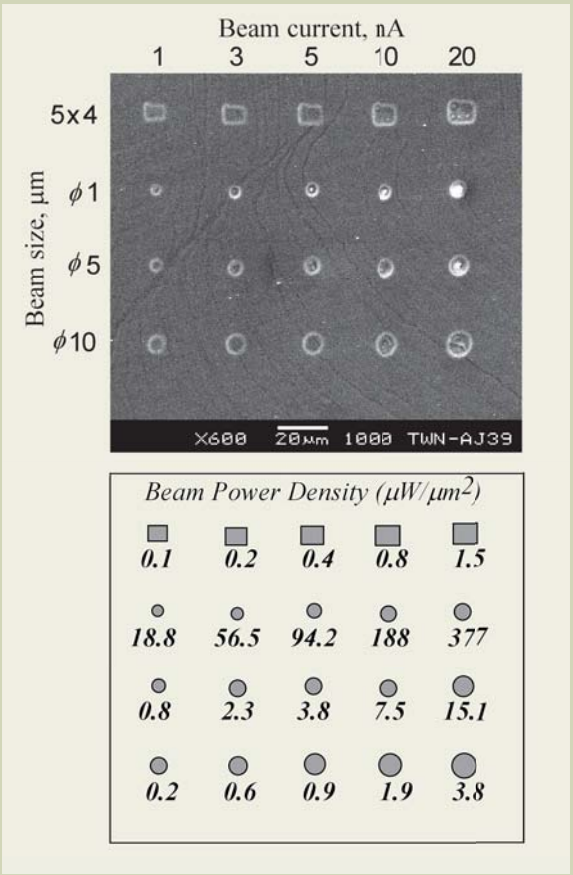

Fig. 1 Examination of beam damage on the polished surface of otolith. (Top) A secondary electron micrograph after the 100 seconds beam exposure with various BPD. Growth increments of otolith are also observed. (Bottom) Legend shows positions of beam spots and their beam conditions. Beam spots at the BPD > 2 μW/μm^2 produced bright pits, which indicate compositional difference compared with surroundings. Severe pitting spots show higher Ca intensity, which may be formed by carbon evaporation of calcium carbonate during beam bombardment. Scale bar: 20 μm.

(2) Selection of the diffracting crystal for target elements

Selection of the X-ray diffraction crystal is based on the highest intensities of the target elements. Both lower and upper sides of background counting positions for each target X-ray line were selected with care to interference peaks using the qualitative line scan analysis. As shown in **Figure 3**, the net intensity of X-ray is calculated with the X-ray baseline intensity. Thus, the height of baseline must be the same between standard materials and otolith. The line scan analysis has been carried out for Ca peak and baseline positions on both Ca and Sr standards, and an otolith.

Counting of Ca $K\alpha$ was made by PETJ crystal

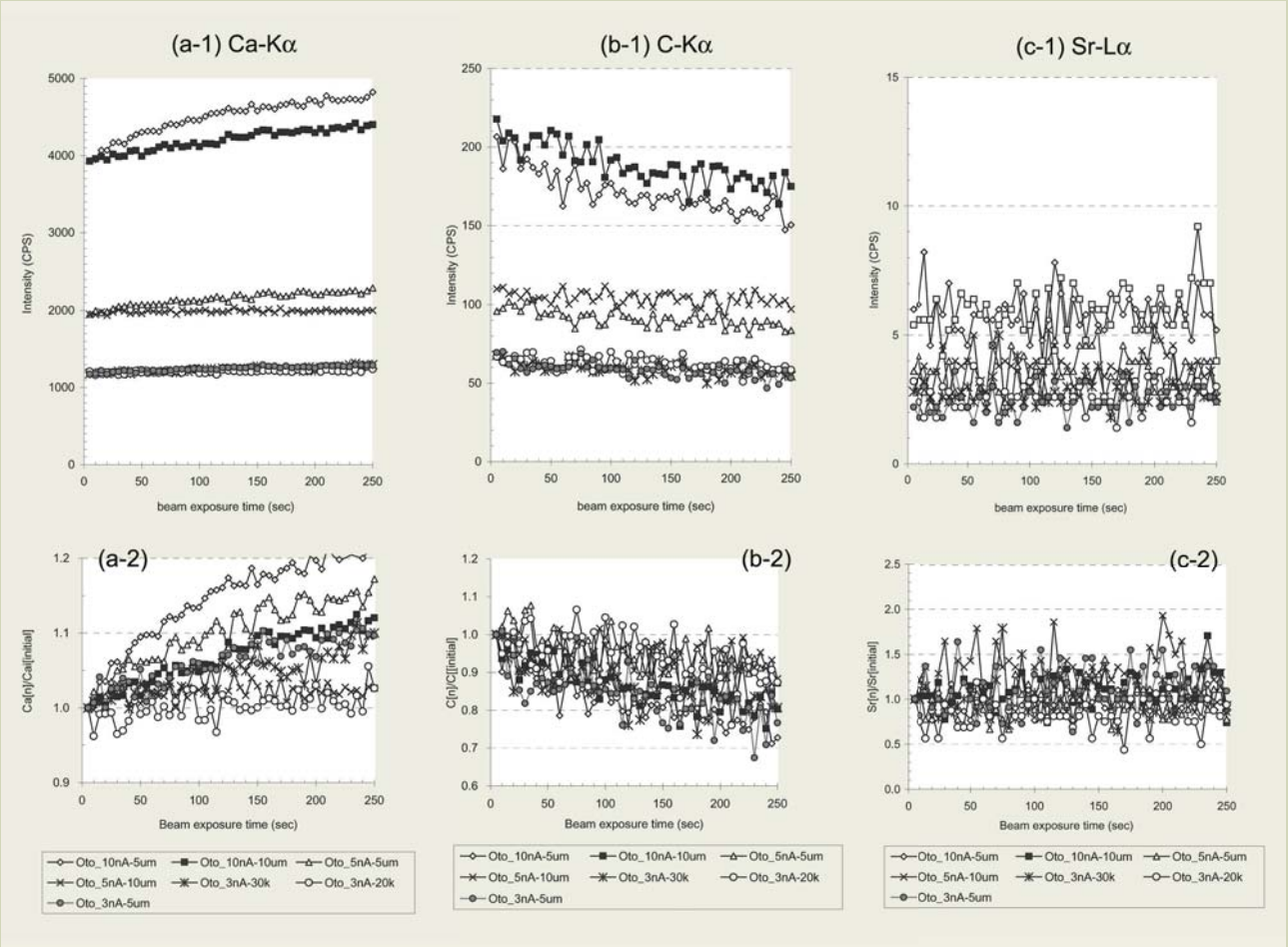

Fig. 2 Transition of X-ray intensities on otolith. Intensities of (a) Ca $K\alpha$, (b) C $K\alpha$, and (c) Sr $L\alpha$ being a function of beam exposure time (sec) at different beam conditions on a Japanese eel otolith. Upper and bottom show alterations of counts and rates of intensities, respectively.

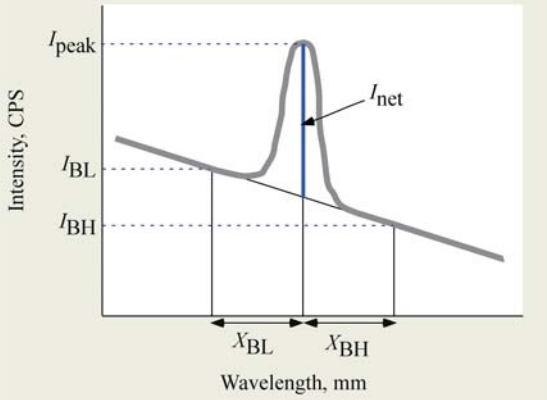

Fig. 3 Measurement of the net peak intensity of target element. I_{bkU} and I_{bkL} are background X-ray intensity (cps) at the positions of upper- and lower side, respectively, and D_{bkU} and D_{bkL} are upper- and lower side distance (in millimeters) of background counting position from the peak position as function of L-values, respectively.

The L-value indicates the distance from the X-ray source (probe spot) to the analyzing crystal. It represents the wavelength detecting position of WDS and is given by the following equation:

$L\ (mm) = [2R/2d]\ n\lambda$

where 2R is diameter of Rowland circle (mm), 2d is spacing of diffracting crystals (Å: angstroms), n is order of reflection, and λ is wavelength (Å).

(**Table 1**). As shown in **Figure 4**, the Ca *Kα* position is isolated with other peaks and there are low-enough baseline both low- and upper-side.

Counting of Sr *Lα* was made by TAP crystal, because intensity of Sr on the TAP is 4-7 times stronger than the intensity on another possible diffracting crystal, such as PET or PETH, at the same beam condition (**Fig. 5** and **Fig. 6**). However, the line scan analysis shows that, Sr *Lα* and Ca *Kα* peaks were observed as interference peaks of the lower side of Sr *Lα* baseline (Fig. 5). In particular case of the Sr standard strontinite, the lower side of baseline was affected by Sr *Lα* peak and their baseline height is 4-5 times higher than both of the Ca-standard aragonite and an otoith baseline (Fig 5-d, e, f). And the position of lower baseline is the same to the lowest limit of TAP, therefore, the TAP is not appropriate to measure

Table 1 An optimum setting of WDS-EPMA to measure Sr/Ca ratios of the otolith.

Machine:			
JEOL EPMA JXA-8900R at the Institute of Earth Sciences, Academia Sinica, Taipei			
Beam conditions			
Acceleration Voltage: 15kV			
Primary beam current: 3nA			
Beam size: $5 \times 4\ \mu m^2$ rectangular scanning beam (×20,000 in magnification)			
Correction method: Oxide PRZ (Phi-Rho-ZAF)			
Analytical condition			
WDS channel	1	3	4
element	Carbon	Strontium	Calcium
Standard material	Aragonite	Strontianite	Aragonite
(formula)	$CaCO_3$	$(Sr_{0.95}Ca_{0.05})CO_3$	$CaCO_3$
WDS setting			
Diffracting crystal	STE	PETH	PET
X-ray Counting position	C *K α*	Sr *L α*	Ca *K α*
Peak position, mm	ca. 124.4	ca. 220.1	ca. 107.5
Background (+), mm	10.5	14.5	5.0
Background (-), mm	8.0	20.0	5.0
X-ray Counting time (total)	50	120	40
Peak, sec	30	80	20
Background (+), sec	10	20	10
Background (-), sec	10	20	10

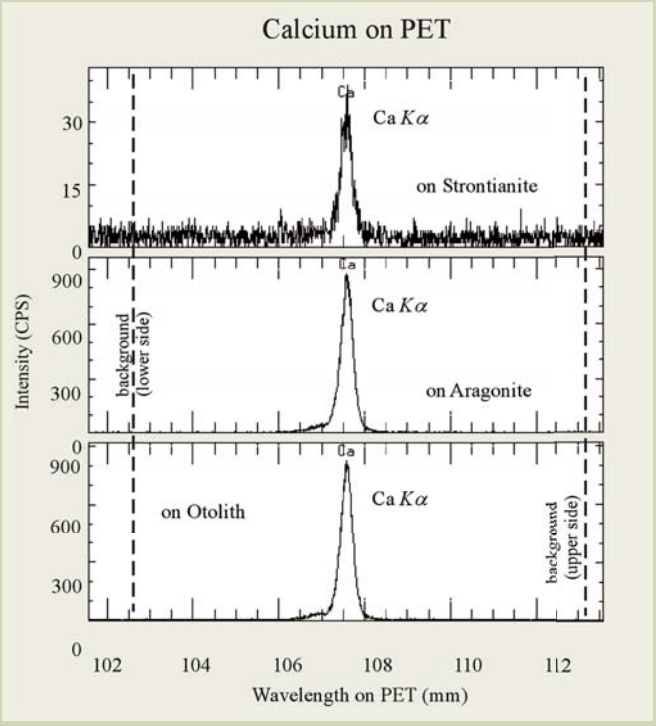

Fig. 4 Scanning of Calcium X-ray intensity on the carbonate standards (strontianite and aragonite) and an otolith, with diffracting crystals PET. The vertical and horizontal axes are X-ray intensity in count per second (cps) and which is shown as the L-value in mm, respectively. Any interference peak was absence around Ca *Kα* peak on the PET crystal. Measurement positions of each baseline, lower- and upper-side were selected on no interferences positions.

Sr. Although the PET is obtained lower intensity of Sr, there is no base line problem and is enough space to avoid interference peaks, such as Sr $L\alpha$ and Ca $K\alpha$ (Fig. 6). The C $K\alpha$ line was interfered by the carbon-coating itself and was shown broad peak, though the intensities of C $K\alpha$ line were strong enough to examine (**Fig. 7**). To determine the above 3-elements, it is selected that double PET are measurements for Ca and Sr, the STE is for C (*see* Table 1).

(3) Effect of exposure time with Ca, Sr, and C intensity at different beam current and beam size

Relations between the X-ray intensities and beam exposure time were determined for Ca $K\alpha$, C $K\alpha$ and

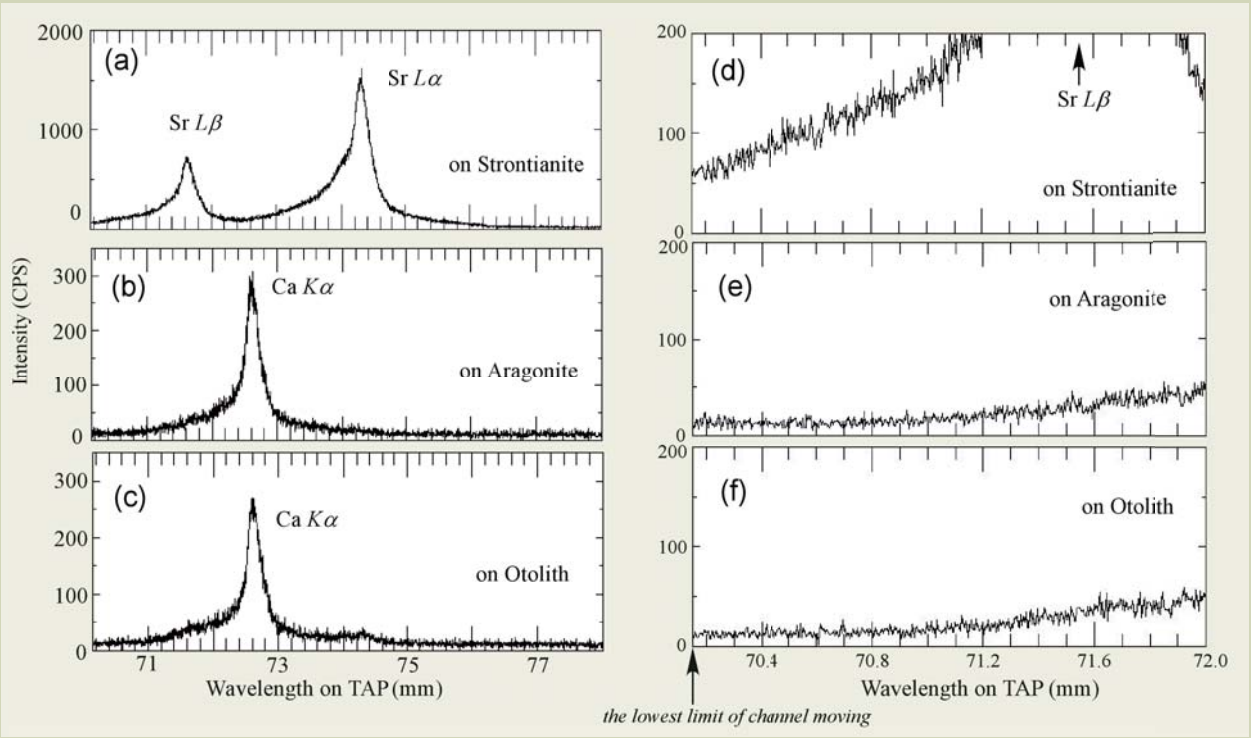

Fig. 5 Scanning of Strontium X-ray intensity on the carbonate standards (strontianite and aragonite) and an otolith, with diffracting crystals TAP. On the TAP crystal, Sr $L\alpha$ on (a) strontianite, and (b) Ca $K\alpha$ on aragonite, and (c) an otolith are observed as interference peaks of Sr $L\alpha$ (target peak), respectively. And baseline heights are considerably different among (d) strontinanite, (e) aragonite and (f) an otolith.

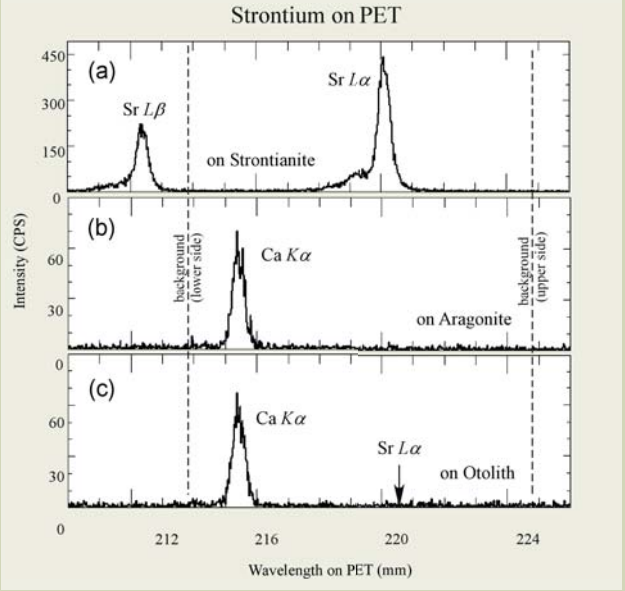

Fig. 6 Scanning of Strontium X-ray intensity on the carbonate standards (strontianite and aragonite) and an otolith, with diffracting crystals PET. Measurement positions of each baseline, lower- and upper-side were selected on no interferences positions.

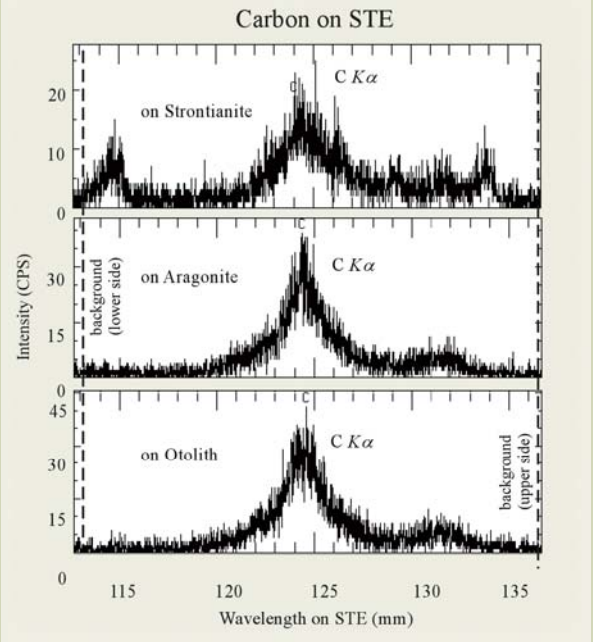

Fig. 7 Scanning of Carbon X-ray intensity on the carbonate standards (strontianite and aragonite) and an otolith, with diffracting crystals STE.

Sr $L\alpha$ of the standards, calcite (**Fig. 8**), aragonite (**Fig. 9**) and strontianite (**Fig. 10**) at the BPD ranging from 0.2 to 7.5 μW/μm^2, as well as on the otolith experiment (Fig. 2). The Ca, Sr and C intensities were counted for 5 sec × 25 cycles at the same spot after setting each peak position. Total beam exposure time is 250 sec at each analysis spot.

The intensities of Ca, C and Sr were greater at higher than lower beam currents (Fig. 8, 9, 10). At higher beam current on calcite and aragonite, the intensities of Ca increased and C decreased with increasing exposure time, and the extent of alteration depended strongly upon the BPD. At the lowest BPD (0.2: 3 nA – 5 × 4 μm^2 rectangle beam), Ca intensities on calcite are slightly increasing with the time (Fig. 8a-1 and 8a-2), though Ca on aragonite did not change throughout the analysis for 250 sec (Fig. 9a-1 and 9a-2). This behavior is also observed in case of otolith time study (Fig. 2). On the other hand, the intensities of C were severely altered under the higher BPD beam compared with that of a larger beam size regardless of beam current (Fig. 8b and 9b). Changes of Sr intensities were smaller than those of other two elements regardless of the BPD and the exposure time (Fig. 10).

These observations indicate that the surface condition of specimen has been modified by the electron beam bombardments, and the extent of alteration depended upon the BPD, primarily beam diameter as well as beam exposure time determined the extent of the alteration. It is not only happened an organic carbonate otolith but also occurred on the inorganic carbonates,

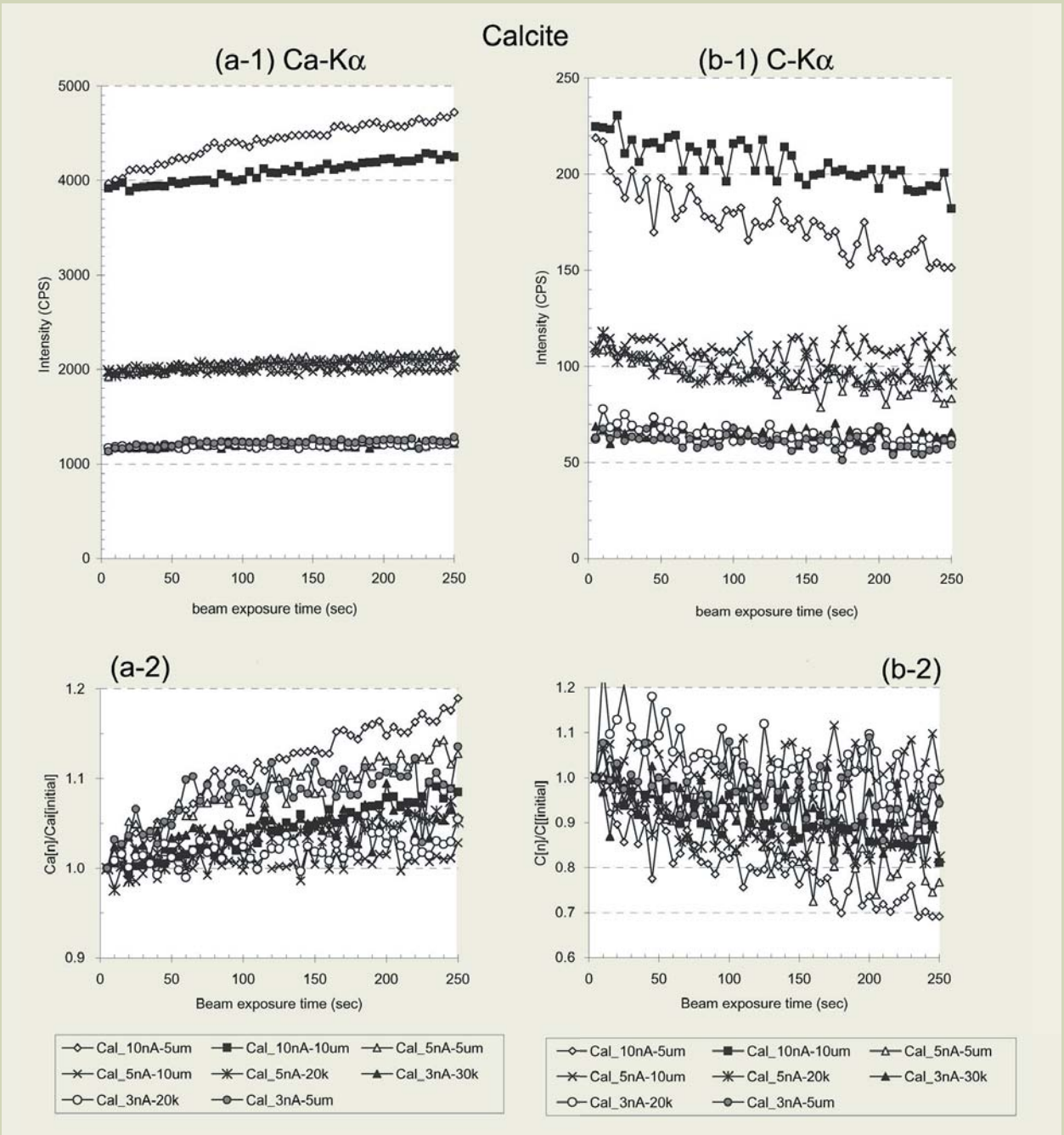

Fig. 8 Intensities of (a) Ca $K\alpha$, and (b) C $K\alpha$ being a function of beam exposure time (sec) at different beam conditions on calcite standard. Upper and bottom show alterations of counts and rates of intensities, respectively.

calcite and aragonite. The changes in intensities of Ca and C with exposure time may be due to changes of the original surface by beam damage within a few minutes of exposure.

During beam exposure for analysis, the entire energy of the incident electron beam is dissipated in the form of heat at the point of impact [19]. The degree of heating is depending upon the BPD and the type of specimen. Casting [24] estimated that the rise in temperature (ΔT, °C) resulting from an electron beam diameter d (μm) and thermal conductivity k (W/cm) of target is given by

$$\Delta T = 4.8\left(\frac{E_0 I}{kd}\right)$$

where E_0 is the incident energy of the electron beam (kV), and I is beam current (μA).

Plotts [20] determined that the temperature rise in lower k minerals, such as calcite (k = 0.05 [25]), and it could be large cause of decomposition and/or structural alteration ($CaCO_3$ -> $CaO + CO_2$). Although there is no report about the thermal conductivity k of aragonite, it is expected that the aragonite-carbonate is also decomposed during the beam heating from the results from Figure 9. The decrease of C intensities might be related with evaporation effect of the CO_2 from the beam spot, and as a result increasing of Ca intensities occurred during beam exposure. It is suggested that the effect of beam damage should indicate wrongly estimation of chemical composition. Thus, the temperature rise on the

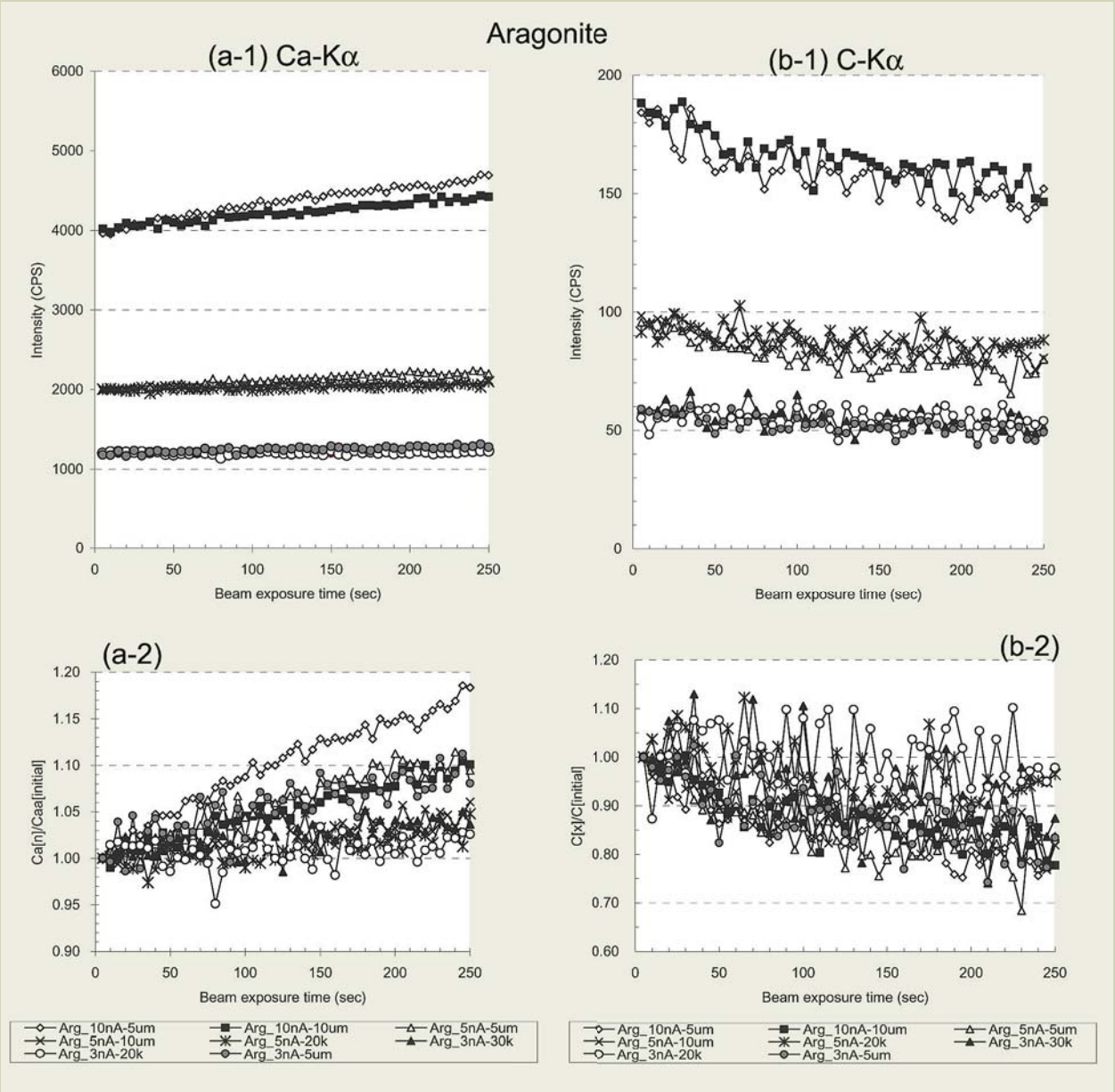

Fig. 9 Intensities of (a) Ca $K\alpha$, and (b) C $K\alpha$ being a function of beam exposure time (sec) at different beam conditions on aragonite standard. Upper and bottom show alterations of counts and rates of intensities, respectively.

surface of otolith should be considered. This indicates that beam damage caused by a high BPD may have led to inaccurate quantifications of otolith chemical composition.

This phenomenon was also suggested by Gunn et al. [15]. And they recommended 1.2 μW/μm^2 in the BPD, which was conducted by 15 kV, 25 nA and 20 μm of acceleration voltage, beam current and diameter, respectively. However, the width of increments, growth rings, of otolith is smaller than a few μm, so that the size of electron beam should be required to reduce as smaller as possible to obtain the special resolution. In some of previous studies, a small beam diameter (smaller than 1 μm) and an extremely high BPD (greater than 100 μW/μm^2) was used to measure Sr/Ca ratios in otoliths. As mentioned previously, a small beam diameter and high BPD may lead to severe otolith surface damage and the alteration of otolioth chemical composition. Subsequently, this could lead low precision and inaccurate quantification of otolith Sr/Ca ratios estimations. Accordingly, a small beam diameter and a high BPD should not be used for measurement of Sr/Ca ratios in otoliths.

To avoid decomposing the sample, various preventive measurements can be applied. The beam current can be reduced or, alternatively, the beam may

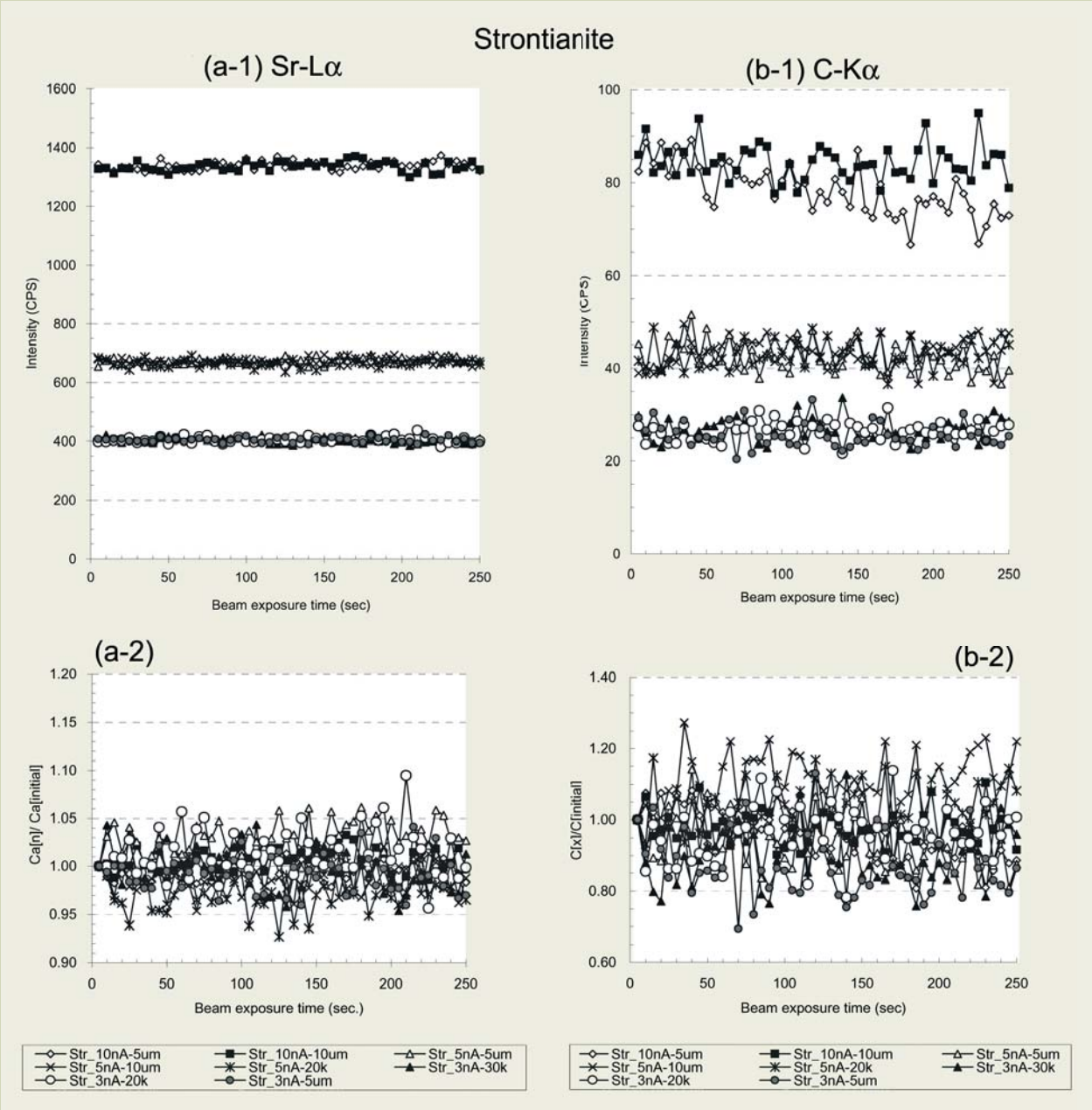

Fig. 10 Intensities of (a) Sr *Lα* and (b) C *Kα* being a function of beam exposure time (sec) at different beam conditions on strontianite standard. Upper and bottom show alterations of counts and rates of intensities, respectively.

be defocused to allow energy dissipation to spread over a larger area. As suggested by the alteration of Carbon under a focused beam, the use of a focused beam less than 1 or 2 μm should be avoided. This does, however, sacrifice spatial resolution. Again that wider electron beam is, on the other hand, inappropriate for analysis of the fine growth increments in otoliths. Consequently, it must be accepted that beam exposure time should be shortened and that beam current and diameter should be as low as possible. Because of these considerations, it is suggested that beam conditions are optimal when the BPD is less than 0.5 μW/μm^2 and beam diameter >2 μm. Note that the lower probe current (less than 1 nA at 15 kV) is not acceptable for the analysis of otolith because of low Sr *Lα* intensity. From the experiment of the effects of BPD on the X-ray intensities of Ca, C and Sr, four beam conditions were found to have a BPD less than 1 or 0.5 μW/μm^2, which appears to minimize damage and therefore are acceptable for the analysis of otolith Sr/Ca ratios. According to the changing of X-ray intensities on both standard and otolith, the optimal beam conditions for the analysis of Sr/Ca ratio in the otoliths is suggested to be 3 nA and 5 × 4 μm^2 beam (BPD = 0.2 μW/μm^2).

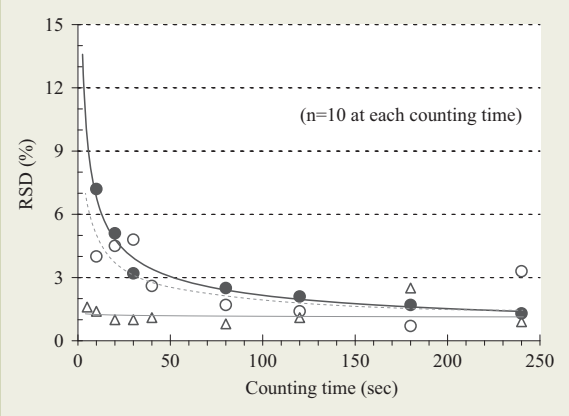

Fig. 11 Accuracy of X-ray counting at different counting time (sec) for Sr *Lα* peak (solid circles), lower side background (open circles), and upper side background (open triangles) on strontianite.

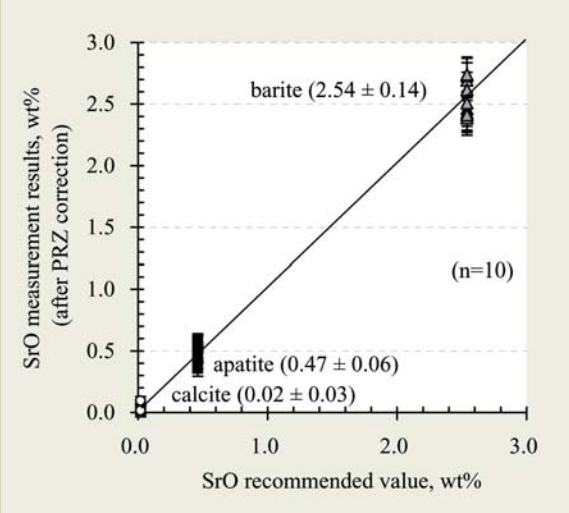

Fig. 12 Correlation between the measurement results and the recommended values of SrO (wt%) of the chemical-known standard materials at the optimum beam condition. Symbol and the recommended value; open circle: calcite (0.02 wt%); solid square: apatite (0.46 wt%); triangle: barite (2.537 wt%). Measurements have been carried out for 10 times on each material and shown mean value and 1σ error in wt%, respectively.

(4) Variability of intensity in relation to exposure time

To confirm the precision of background counting in the function of counting time, the smallest detectable peak was defined. Additionally, to achieve an appropriate counting time for Sr in the quantitative otolith analysis, precision of peak analysis was examined using the standards at conditions of the lowest BPD (0.2 μW/μm^2: 3 nA and 5 × 4 rectangle beam) on the Sr-standard strontianite. The beam exposure time on each counting was set from 10 to 240 sec. The X-ray intensity was measured from 10 different points.

The relative standard deviation (RSD) of X-ray intensities of Sr in relation to beam exposure time is shown in **Figure 11**. The RSD of both lower- and upper-side backgrounds decreased gradually from 5 % to less than 2 % with an increase in the exposure time. The RSD of the Sr peak decreased gradually from 7 % to 3 % with increasing exposure time up to 80 sec. However, at an exposure time longer than 180 or 240 sec, the RSD of baselines slightly increased, indicating that the X-ray intensities are altered if exposure times exceed 180 or 240 sec even at lower BPD. Whereas the precision of Ca analysis were <0.5 % RSD, regardless of the beam conditions, at an exposure time between 20 and 40 sec. Because Ca can be measured simultaneously with Sr by multiple WDS channels, total analysis time including peak and background counting should be considered only for Sr analysis. Therefore, it is desirable that the total analysis time was restricted less than 180 sec for each spot, and peak-counting time should be between 80 and 120 sec, and as result the each background-counting time should be between 20 and 30 sec.

(5) Precision of Sr measurement in otolith

The sagittal otolith generally contain less than 1 wt% of Sr. However, it must be used higher Sr content standard (strontianite: Sr = 59.4 wt%) because it is unable to find a low-concentration and homogeneous material of the carbonate matrix. To confirm the precision of Sr analysis, Sr contents were measured with the beam current of 3 nA and 5 × 4 μm^2 beam, and the peak and bases counting times were 80 sec and 20 sec, respectively (so called *an optimum beam condition*), using chemical-known materials, calcite, apatite and barite. The results and analytical reproducibility ($1\sigma_{mean}$) of SrO are shown in **Figure 12**. The measured and recommended SrO (wt%) was highly linearly correlated (r = 0.991).

The Sr contents in the otolith and their measurement precision were quantified using the *optimum beam condition*. Sr contents were measured from 5-points at 4-different increments of the otolith under the electron

image. The relation between the net peak intensity of Sr, and Sr analysis result, which after corrected by the PRZ, are shown in **Figs. 13** and **14**, and **Table 2**. The standard deviation (SD) of Sr in otoliths in CPS (count per second) were obtained to be 0.29 cps at the highest net intensity of 3.8 cps (RSD = 7.6%; no.4 in Table 2), and 0.22 cps at the lowest net intensity of 0.9 cps (RSD = 24.4%; no.1). These error ranges were computed for the precision of Sr contents in otolith; Sr = 0.14 ± 0.03 wt% (no.1), 0.33 ± 0.04 wt% (no.2), 0.46 ± 0.05 wt% (no.3) and 0.61 ± 0.05 wt% (no.4). Assuming that Ca contents in otoliths were 39.0 wt%, Sr/Ca ratios in eel otoliths were estimated to be $3.59 \pm 0.77 \times 10^{-3}$ (no.1), $8.46 \pm 1.03 \times 10^{-3}$ (no.2), $11.79 \pm 1.28 \times 10^{-3}$ (no.3), and $15.64 \pm 1.28 \times 10^{-3}$ (no.4), respectively. If it is assuming maximum error of Ca (RSD < 1.0%), the ranges of error in Sr/Ca ratios are smaller than these estimation.

Study of migratory behavior and habitat of three major temperate species of eels by otolith microchemistry

Most of fishes migrate with various spatiotemporal orders. Classification of fish migration is divided into two types. Diadromous fishes migrate between fresh- and sea- or brackish-water, whereas non-diadromous fishes migrate within freshwater (e.g., carp) or seawater environment (e.g., tuna). Diadromous fishes are, further, divided into 3-types; anadromous, catadromous and amphidroumous. Anadromous fishes are spawning in the freshwater river and grown in seawater (e.g. salmon). Catadromous fishes are spawning in seawater and grown in freshwater (e.g., eel), and amphidroumous fishes migrate between sea- and fresh-water bodies frequently (e.g., sweetfish "*ayu*" and smelt "*shi-sya-mo*").

Catadromous eels are widely distributed in the world. In particular, three major temperate species, Japanese eels *Anguilla japonica* in the East Asia, American eels *Anguilla rostrata* in the Northeast America, and European Eel *Anguilla anguilla* in the West to Northwest Europe and North Africa are valuable for economy, aquaculture and fishery (**Fig. 15**). Habitat of Japanese eel is in the NW Pacific Ocean, and is found in brackish water lakes and estuaries and freshwater rivers from southern Taiwan to Japan in Northeastern Asia. Their leaf-like larvae, *leptocephali*, drift with the North Equatorial Current and Kuroshio from their oceanic spawning grounds, near the Mariana Islands, to the continental shelf of northeastern Asian countries [13, 26, 27]. In the Atlantic, on the other hand, American and European eels spawn in the Sargasso Sea and migrate along the Gulf Stream for the East Coast of North America and the West to Northwest Europe and North Africa. They then metamorphose into transparent glass eels in coastal waters and become pigmented elvers in the estuary. After upstream migration, the elvers become yellow eels and live around estuary and in freshwater rivers for approximately 5 to 20 years [8, 12, 28], and then, once they have reached sexual maturity, migrate downstream to the open ocean to spawn.

Otolith microchemistry is a good tool to indicate migration pattern from individual fish. Patterns of otolith Sr/Ca ratios from core to edge illustrate eel's movement. Since the last decade, more than 1000 otoliths have been studied from the difference water bodies (Fig. 15). In this section, results of application studies on three major temperate species of eels are presented.

(1) Analytical procedure

Sagittae, the biggest of the 3 pairs of otoliths, were removed from the inner ear for examination of microchemistry. The procedure of otolith preparation for the analysis of Sr and Ca is similar to Tzeng et al.

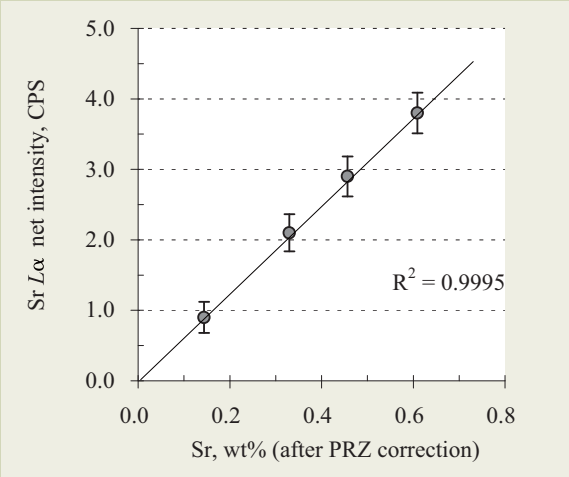

Fig. 13 Correlation of Sr $L\alpha$ intensities (CPS: counts per second) and Sr concentrations (wt% after PRZ correction) on otolith samples.

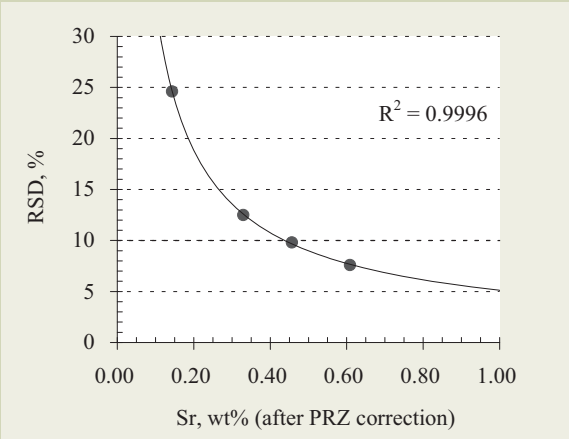

Fig. 14 Estimated RSD (Relative Standard Deviation) of Sr measurements, which obtained by the optimum beam condition.

Table 2 Sr measurement accuracy of otolith.

	Sr, wt%	measured CPS	S.D. (CPS)	S.D. (%)	Sr error in wt%
1	0.14	0.90	0.22	24.6	±0.03
2	0.33	2.10	0.26	12.5	±0.04
3	0.46	2.90	0.28	9.8	±0.05
4	0.61	3.80	0.29	7.6	±0.05

CPS: count per second, S.D.: standard deviation (1σ).

[13]. The sagittal otolith was cleaned with distilled water, air dried, embedded in epoxy resin, ground and then polished along the sagittal plane with alumina compound until the primordium (core) was exposed. All specimens were cleaned with distilled water again in an ultra-sonic bath and air dried before the carbon coating. coating.

Concentrations of both Sr and Ca in otoliths were measured using *the optimum beam conditions* (Table 1) along a sagittal section from the primordium (core) to the otolith edge at an interval of 10 μm (**Fig. 16**). After the EPMA study, growth increments of most of otolith were counted for age determination.

(2) Migration patterns of Japanese eels in Taiwan

To understand the environmental history of the Japanese eel after migration from off shore spawning

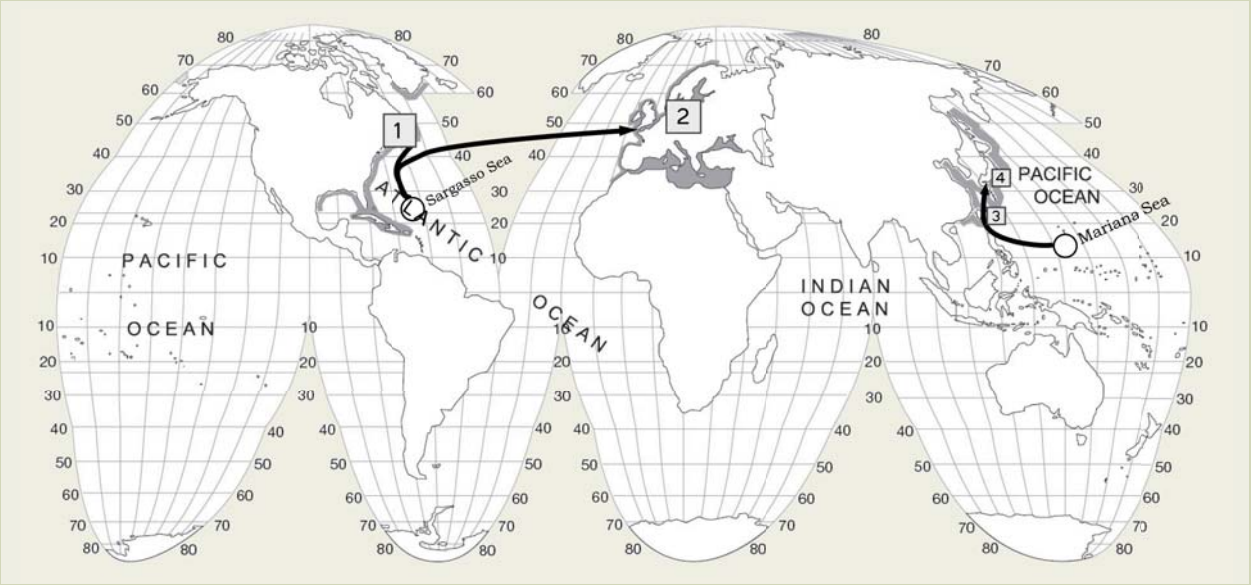

Fig. 15 Main study fields showing the geographical range of each species [35]: American eel *Anguilla rostrata*, (1) New Brunswick, Quebec, and Nova Scotia, Canada [13, 30, 36-41]; European eel *A. anguilla* (2) Baltic Sea region, Sweden, Lithuania and Latvia [32, 33, 42-44]; Japanese eel *A. japonica*, (3) Taiwan; and (4) Japan [14, 28, 29]. Solid lines and open circles represent expected paths of upstream migration (with the Gulf Stream in the Atlantic and the Kuroshio Current in the Pacific), and spawning sites (Sargasso Sea in the Atlantic and Mariana Sea in the Pacific), respectively.

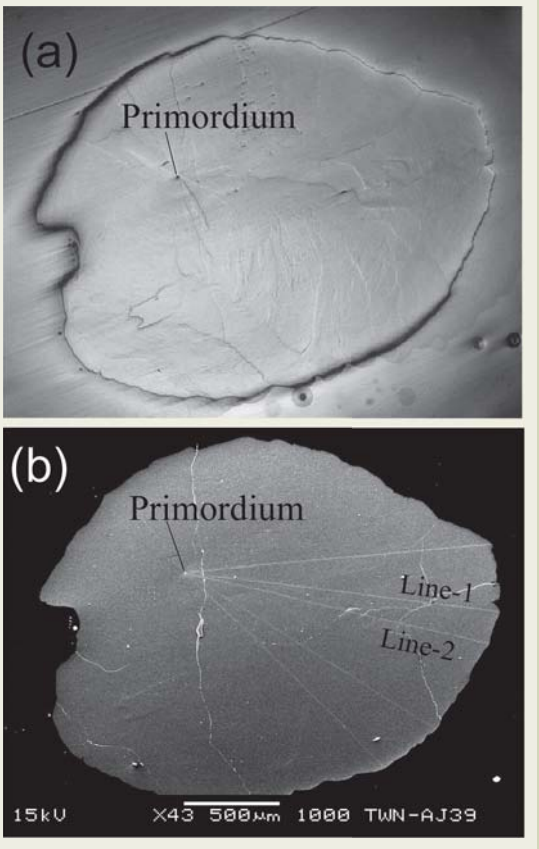

Fig. 16 (a) Optical micrograph of a polished otolith. (b) Secondary electron micrograph of polished surface of otolith after the transect analyses with 10 μm intervals. Analytical tracks are observed as thin-white lines on the surface. Obtained results from Line -1 and -2 are shown in Fig. 17-c (sample D-39).

grounds to estuaries, the temporal change of Sr/Ca ratios in otoliths of eels collected several estuary areas in southwestern Taiwan were examined. A total of over 200 otoliths were measured and the results have been reported [14, 28, 29]. Among them, four typical migratory patterns were described (**Fig. 17**). Selected four otoliths of Japanese eels from Taiwan were examined with two lines to confirm reproducibility of analysis as well. The ratios on lines #1 and #2 of the same otolith were identical at the same distance from the core, indicating that the analytical precision was acceptable to discussion. During the *leptocephalus* marine stage of early life, Sr/Ca ratios were similar among individuals and increased from 6-10 × 10^{-3} (Sr contents: approx. 0.2-0.4 wt%) in the core to approximately 16-18 × 10^{-3} (Sr: approx. 0.6-0.8 wt%), an initial peak at a distance 60-100 μm from the core. Subsequently, decreases once to approximately 7 × 10^{-3} (Sr: <0.3 wt%) were detected in all of the otoliths (Fig. 17). This indicates that the environmental history of the *leptocephalus* stage was similar among individuals. However, beyond the *leptocephalus* stage the Sr/Ca ratios dropped to below 1 × 10^{-3} (Sr: <0.05 wt%) in first half of otoliths T-54, T-21 and D-39 (Figs. 17a, 17b and 17c), whereas the ratios in otolith T-27 dropped to an intermediate level of 3.5 × 10^{-3} (Sr: 0.14-0.16 wt%: Fig. 17d). These measurements were detected at a distance of 180-210 μm from the core. Following the initial drop, Sr/Ca ratios in the otolith of T-54 remained at less than 4 × 10^{-3} (Sr: <0.15 wt%) until the otolith edge. The otoliths of T-21 and D-39 showed a different pattern where ratios increased from a lower level of 4 × 10^{-3} and reached a secondary peak of 8-12 × 10^{-3} (Sr: approx. 0.3-0.5 wt%). Ratios at the second peak were lower than that of the initial peak in the core area, and continued to gradually decrease. The Sr/Ca ratios in the otolith of T-27, on the other hand, did not decrease as low as others, and the ratios remained at a relatively higher level of 6-10 × 10^{-3} (Sr: 0.3-0.4 wt%).

These observations indicate that the Sr/Ca patterns beyond the initial peak can be roughly divided into 4 types (**Fig. 18**); namely, Type A: the Sr/Ca ratios decreased to a lower level (< 4 × 10^{-3}) and remained at that level there-

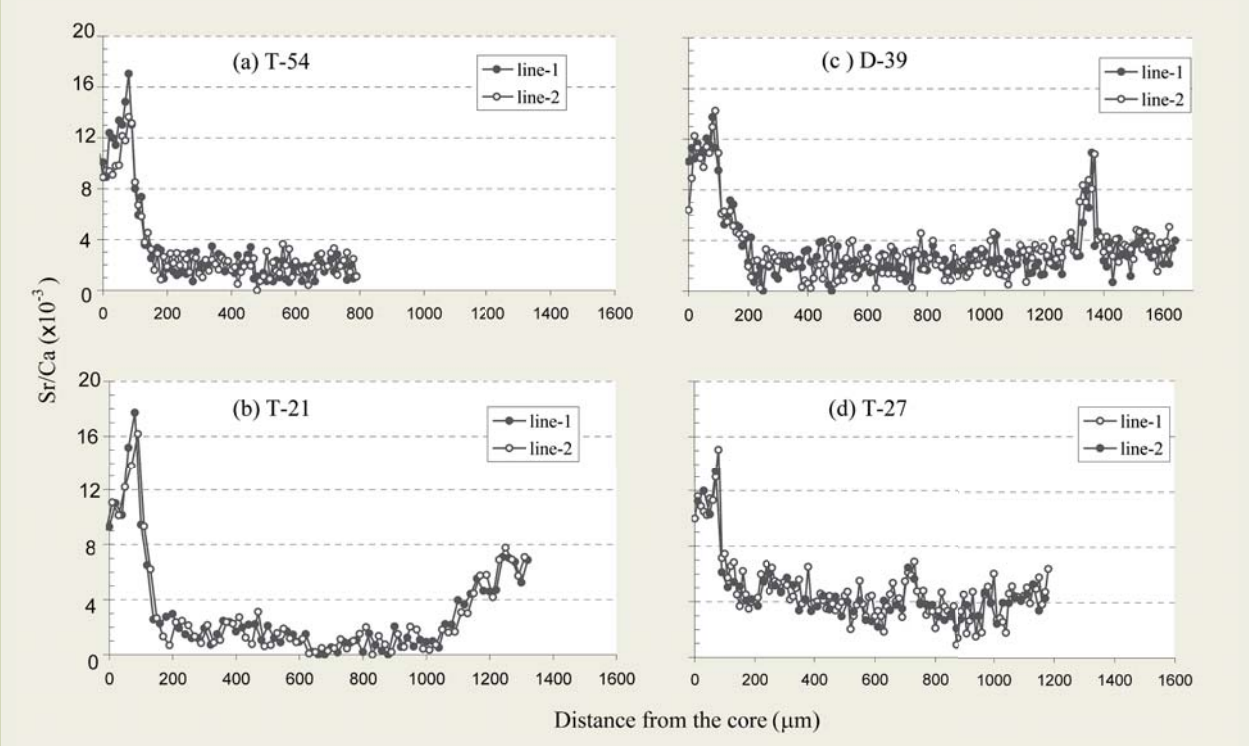

Fig. 17 Sr/Ca ratios determined on 2 parallel transect lines from the primordium to the edge in otolith. The vertical and horizontal axes are Sr/Ca ratio (×10^{-3}) and distance from the primordium. Interval of analysis spot is 10 μm. [14, 28, 29].

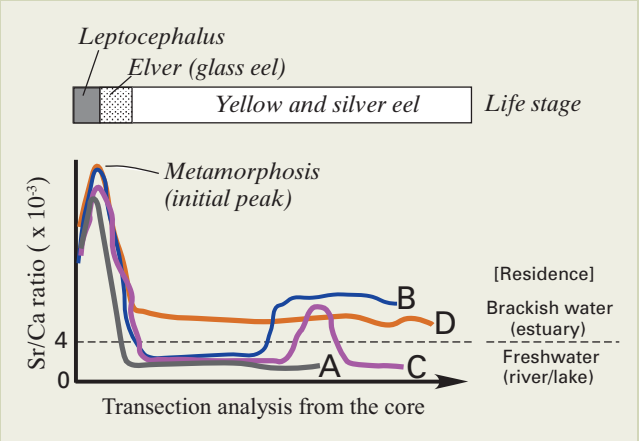

Fig. 18 Schematic diagram of migration patterns of Japanese eels in Taiwan as indicated by the time series change of Sr/Ca ratios in otoliths. Transition of freshwater and brackish water residence is suggested be approximately 4 × 10^{-3} in Sr/Ca ratio.

after; Type B: the ratios decreased in a manner similar to those of Type A, but increased to the secondary peak of approximately 6-10 × 10^{-3}; Type C: the ratios decreased and increased in a manner similar to those of Type B, and decreased to the lower ratio again; Type D: the ratios did not decrease to a level as low as others type, and remained between 1 and 6 × 10^{-3}. According to the Sr/Ca patterns and their captured records of eels, each pattern indicates different migration histories as follows; Type A: a freshwater residence; Type B: An amphdroumous behavior as residence in freshwater, and shifted brackish water residence; Type C: An amphdroumous behavior as residence in freshwater, and shifted brackish water residence, then freshwater residence again; TypeD: a brackish water residence.

(3) Migration patterns of American eels in Northeast Canada

The Sr/Ca ratio transects along the otolith radius, from core to edge, illustrating 6 life-history patterns determined by otolith Sr/Ca ratio analyses on 162 American Eels *Anguilla rostrata* captured the St. Jean River watershed (lat. 48°N) in Quebec (Canada). Among the 162 eels sampled, we predominantly observed an amphidromous migratory pattern (42%) during the yellow-stage growth phase, followed by brackish (38%) and freshwater (20%) residence behavior. Six type are described as follows: Type-FR (**Fig. 19**-a): Residence in freshwater. Entrance in freshwater between Year 1 (elver mark) and Year 2. Type- BR (Fig. 19-b): Residence in brackish habitat (for eel [b] otolith was not clear enough to allow a correct age determination). Amphidromous behaviors are divided into 3 groups, namely, Type-A_{BF} (Fig. 19-c): Residence in brackish environment for more than 2 yr, then movement into freshwater. Type-A_{FB} (Fig. 19-d): Residence in freshwater then movement to brackish habitat. Type-A_{FBF} (Fig. 19-e): Freshwater residence, movement to brackish estuary then movement to freshwater. And Type-A_{ND} (Fig. 19-f):

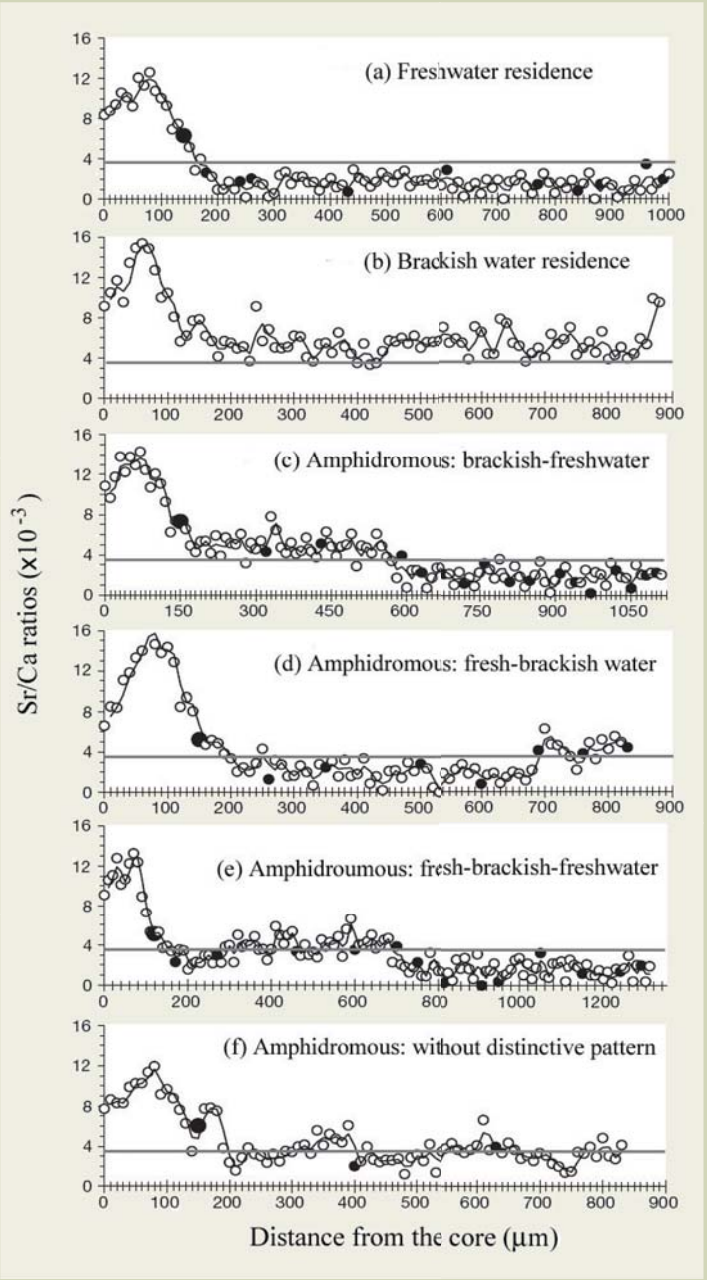

Fig. 19 Representative migratory patterns of American eels *Anguilla rostrata* from St Jean River watershed in Quebec (Canada). The Sr/Ca ratio transects along the otolith radius, from core to edge, illustrating 6 migratory patterns: (a) Type-FR: freshwater residence [sample # IT-206], (b) Type-BR: brackish water residence [# IT-061], (c) Type-A_{BF}: amphidroumous [brackish-freshwater: # IT-285], (d) Type-A_{FB}: amphidroumous [freshwater-brackish: # IT-014], (e) Type-A_{FBF}: amphidroumous [freshwater-brackish-freshwater: # IT-211], (f) Type-A_{ND}: amphidroumous [non distinctive pattern: IT-116]. The Sr/Ca ratio patterns were interpreted point-by-point from the elver check to the otolith edge with 2-point smoothed averages, according to a threshold of 3 to 4 × 10^{-3} between fresh and brackish water bodies, shown as thin straight line. Small solid circles represent annuli. The first peak of Sr/Ca ratio before 100 µm corresponds to metamorphosis from leptocephalus to glass eel of Japanese eels (see Figs. 17 and 18). Amphidromous migratory patterns are predominantly observed (42%) during yellows eels stage among the studied 162 eels, followed by brackish (38%) and freshwater (20%) residence behavior [30].

Frequent movements between habitats, with no defined. A threshold between fresh and brackish water masses is of 3-4 × 10^{-3}. The Sr/Ca ratio peak observed before 100 µm corresponds to metamorphosis from *leptocephalus* to glass eel [30]. Sr distribution mapping for the six typical otoliths are shown in **Figure 20**. The core areas are surrounded by highest Sr content (red in color). Scale in each map: 200 µm.

(4) Different Sr/Ca patterns of European eels in the Baltic Sea area

Intensive stocking programs have been undertaken in the Baltic Sea region over the past 50 years. The most intense stocking programs have been implemented in the Baltic Sea drainage using eels originating from Western Europe. The first eel stockings in Lithuania occurred between 1928 and 1939 when 3.2 million elvers were released into inland freshwater lakes of the Vilnius region (approx. 300 km from the Baltic coast). Since the mid 1960s, Lithuanian lakes have been stocked with approx. 50 million elvers or young yellow eels at an average stocking rate of 1.1 million eels yearly [31]. Studies on stocking effectiveness as well as studies on natural recruitment, however, have not been carried out and the post-stocking movements of stocked eels

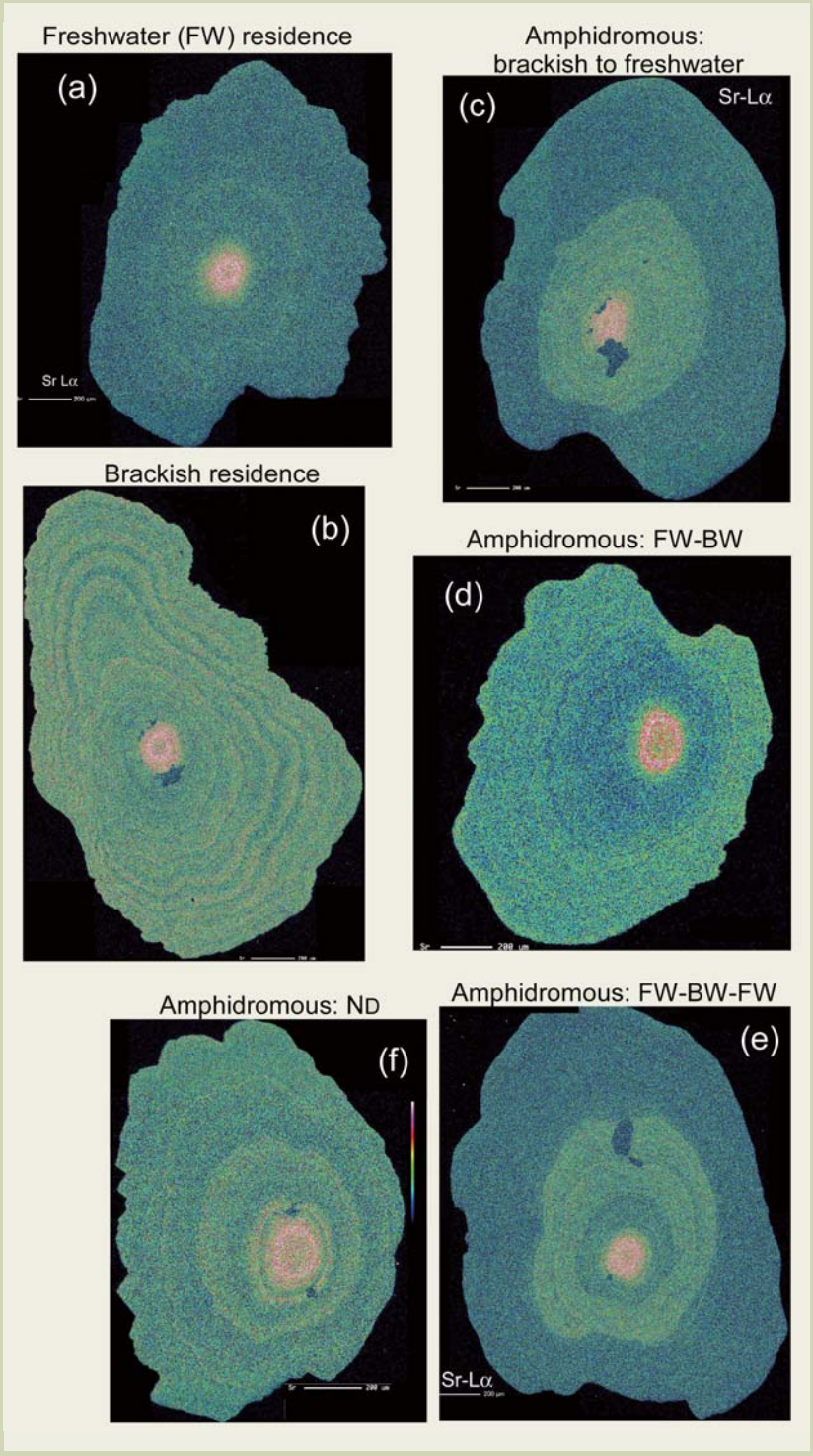

Fig. 20 Sr distribution of sagittal otoliths. Sr *Lα* mapping were performed with TAP diffracting crystal at the condition of 15 kV and 80 nA for the acceleration voltage and beam current, respectively, with 1 µm defocused beam. X-ray intensities were counted for 0.040 sec at the interval of 1 µm. (a) Type-FR (IT-206: Fig. 19-a), (b) BR (IT-061: Fig. 19-b), (c) Type- A_{BF} (IT-285: Fig. 19-c), (d) Type-A_{FB} (IT-014: Fig. 19-d), (e) Type-A_{FBF} (IT-211: Fig. 19-e) and (f) Type-A_{ND} (IT-116: Fig. 19-f). Scale bar is 200µm. Warm color (red) and cold color (blue) are indicate higher and lower concentration of Sr, respectively.

remain largely unknown because of the dissolution of the Soviet Union.

From a series of otolith study of European Eel *Anguilla anguilla* from Lithuanian water body, the Sr/Ca ratio transects along the otolith radius, from core to edge, illustrating 2 significant life-history patterns, multiple migration patterns were observed as well as Japanese and American eels though [32]. As shown in **Figure 21**-a, a solid line represents the mean ± SD (standard deviation) otolith Sr/Ca ratio profile of 20 eels that showed a gradual decline pattern, indicating the movement from the full strength of salinity in the North Sea into brackish water of the Baltic Sea (Phase I: mean Sr/Ca ratio 5.51 ± 1.57 $\times 10^{-3}$) and ultimately arrived at the coastal waters of Lithuania (Phase II: mean Sr/Ca ratio 3.64 ± 1.10 $\times 10^{-3}$). And transition of freshwater and sea/brackish water residence is indicated as 2 to 3 $\times 10^{-3}$ in Sr/Ca ratio. An example which has been studied by Sr/Ca pattern and Sr mapping is shown in **Figure 22**. It is supposed one of typical pattern of the Baltic Sea migration. In Figure 21-b, on the other hand, the mean patterns indicate consistently low otolith Sr/Ca ratios (0.72 ± 0.76 $\times 10^{-3}$) after the glass eel stage from 16 eels which were collected from freshwater lagoon and lake, the Curonian Lagoon (n=6) and Lake Baluošai (n=10). Since their patterns lack the Baltic Sea migration, it is concluded that these patterns are typical from restocked eels. The Sr/Ca patterns indicate the transition from sea/brackish water to freshwater, freshwater residences [32, 33, 43].

Conclusive remarks

Many interpretations of geographical and population genetic studies of fish suffer from uncertainty arising from artificial stocking or due to lack of information about the migrating behavior of species of interest. Successful fish stock management, as well as conservation program are not effective without a complete understanding of the population genetic structure, stock boundaries and spatial and temporal migratory patterns. In recent years, advances in analytical techniques have led to the use of otolith microchemistry as an aid to stock discrimination in fishes. A contribution of EPMA technique based on geo- and mineral chemistry is remarkable. EPMA study of Sr/Ca ratios of otolith can interpret their migration and habit and are now one of most important data.

Genetic markers are widely used as implements for acknowledging potential stock differences. The recent developments of such investigation methods as the assay of microsatellites have provided us with the opportunity to evaluate relationships between populations and subpopulations. By combining two modern techniques; otolith microchemistry and microsatellite DNA analysis, we intend to demonstrate the effectiveness of such an approach to the diadromous fish stocks management [34]. The techniques will present an innovative approach to address the management-related problems and conservation of endangered species.

Acknowledgments

This series of otolith study was conducted with financial support from the Institute of Earth Scineces, Academia Sinica and the National Science Council of Taiwan. The author deeply appreciates Drs. Wann-Nian Tzeng, Jen-Chieh Shiao of National Taiwan University and Dr. Chih-Wei Chang of National Museum of Marine Biology & Aquarium (Taiwan) for their initiation of otolith analysis and discussion. I also thank Drs. Brian M. Jessop and David K. Cairns of Bedford Institute of Oceanography (Canada), Dr. Linas Ložys of Vilnius University (Lithuania), and Dr. Julian J. Dodson of Universite Laval (Canada) for their long term collaborations.

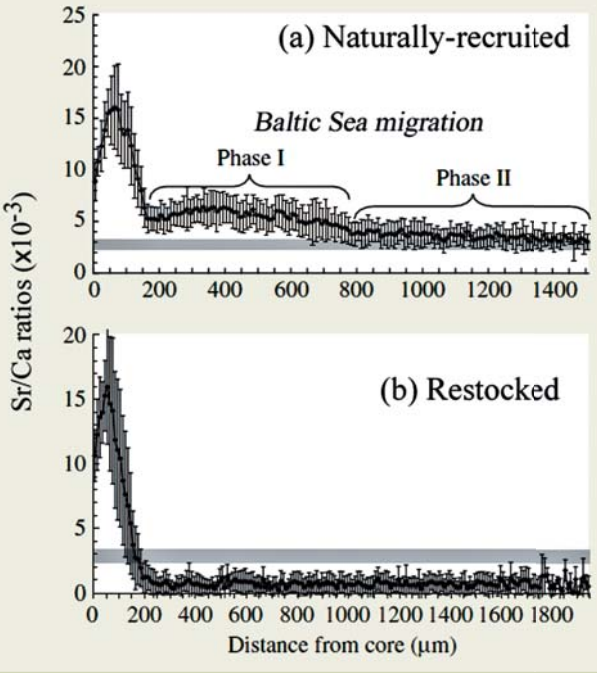

Fig. 21 Comparison of mean value of Sr/Ca ratios of otolith of (a) naturally-recruited and (b) restocked eels from Lithuania water bodies [32]. The transition of freshwater and sea and brackish residence (▮) is indicated. (a) The mean ± S.D. (standard deviation: 1σ) otolith Sr/Ca ratio profile of 20 European eels that showed a gradual decline pattern, indicating the movement from the full strength of salinity in the North Sea into brackish water of the Baltic Sea (phase I: numbers of probe spots = 1240) and ultimately arrived at the coastal waters of Lithuania (phase II: n = 1119). (b) Transects of mean ± S.D. otolith Sr/Ca ratios from 16 freshwater-resident eels, illustrating consistent low values after the glass eel stage.

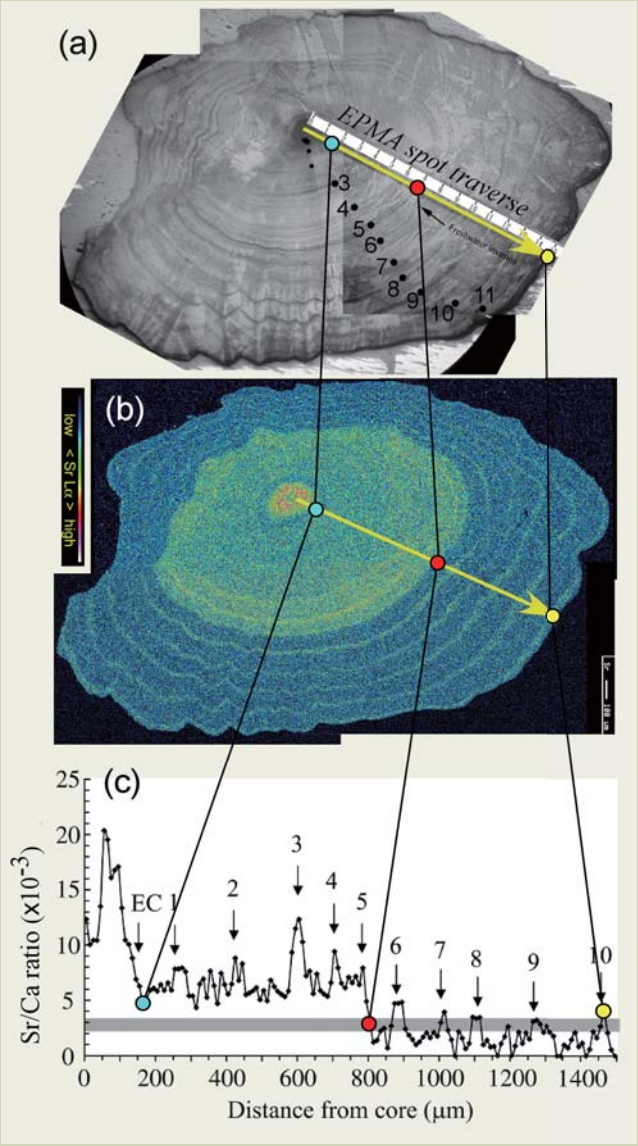

Fig. 22 Otolith Sr/Ca ratio from core to edge illustrates eel movement into fresh water after a period of seawater and brackish-water residence. (a) An optical micrograph of otolith of European Eel *Anguilla anguilla* (Lithuanian eel sampling code LT-1, age 11years old), collected from the Curonian Lagoon in Lithuania (Lat. 56° N). Dots and numbers represent annual increments and estimated ages, respectively. A track of EPMA quantitative transecting analysis from the primordium (core) to edge is shown as a yellow arrow. (b) Sr distribution mapping displays higher Sr content (green in color) from age 1 to 5 years and high Sr rings at annuli 6–10 between age 6 and 11 years (light blue in color) which is assumed as winter marks. The Primordium (core) area is surrounded by highest Sr content (orange in color) and a yellow arrow shows direction of quantitative transecting analysis (c) An example of the Baltic migration pattern Sr/Ca ratios transect along the otolith radius, from core to edge with 10μm interval. A freshwater entry (a red circle) is observed the age between 5 and 6 years old. Seasonal migration between high salinity (a yellows circle) and low salinity or fresh waters is also observed after the freshwater entry. #1–10: the annuli corresponding to peaks in the otolith Sr/Ca ratios; EC: elver check (a blue circle). The transition of freshwater and sea/brackish residence (▇) is indicated [32].

References

[1] Campana SE (1999) Chemistry and composition of fish otoliths: pathways, mechanisms and applications. *Mar Ecol Prog Ser* **188**: 263-297.

[2] Carlstrom D (1963) A crystallographic study of vertebrate otoliths. *Biol Bull* **125**: 441-463.

[3] Degens ET, WG Deuser, RL Haedrich (1969) Molecular structure and composition of fish otolith. *Mar Biol* **2**: 105-113.

[4] Amiel AJ, GM Friedman, DS Miller (1973) Distribution and nature of incorporation of trace elements in modern aragonite corals. *Sedimentology* **20**: 47-64.

[5] Tzeng WN (1996) Effects of salinity and ontogenetic movements on strontium:calcium ratios in the otoliths of the Japanese eel, *Anguilla japonica*. *J Exp Mar Bio Ecol* **199**: 111-122.

[6] Radtke RL (1989) Strontium-calcium concentration ratios in fish otoliths as environmental indicators. *Comp Biochem Physiol* **92A**: 189-193.

[7] Otake T, T Ishii, M Nakahara, R Nakamura (1994) Drastic changes in otolith strontium/calcium ratios in leptocephali and glass eels of Japanese eel *Anguilla japonica*. *Mar Ecol Prog Ser* **112**: 189-193.

[8] Tzeng WN, YC Tsai (1994) Changes in otolith microchemistry of the Japanese eel, *Anguilla japonica*, during its migration from the ocean to the rivers of Taiwan. *J Fish Biol* **45**: 671-683

[9] Arai T, T Otake, K Tsukamoto (1997) Drastic changes in otolith microstructure and microchemistry accompanying the onset of metamorphosis in the Japanese eel *Anguilla japonica*. *Mar Eco Prog Ser* **161**: 17-22.

[10] Thorrold Sr, CM Jones, SE Campana (1997) Response of otolith microchemistry to environmental variations experienced by larval and juvenile Atlantic croaker (*Micropogonias undulates*). *Limnol Oceanogr* **42**:102-111

[11] Kawakami Y, N Mochioka, K Morishita, T Tajima, H Nakagawa, H Toh, A Nakazono (1998) Factors influencing otolith strontium/calcium ratios in *Anguilla japonica* elvers. *Environ Biol Fish* **52**: 299-303.

[12] Tsukamoto K, I Nakai, WV Tesch (1998) Do all freshwater eels migrate? *Nature* **396**: 635-636.

[13] Tzeng WN, KP Severin, H Wickström (1997) Use of otolith microchemistry to investigate the environmental history of European eel *Anguilla anguilla. Mar Ecol Prog Ser* **149**: 73-81.
[14] Shiao JC, Y Iizuka, CW Chang, WN Tzeng (2003) Disparities in habitat use and migratory behavior between tropical eel *Anguilla marmorata* and temperate eel *A. japonica* in four Taiwanese rivers. *Mar Ecol Prog Ser* **261**: 233-242.
[15] Gunn JS, IR Harrowfield, CH Proctor, RE Thresher (1992) Electron probe microanalysis of fish otoliths - evaluation of technique for studying age and stock discrimination. *J Exp Mar Biol Ecol* **158**: 1-36.
[16] Sadovy Y, KP Severin (1992) Trace elements in biogenic aragonite: Correlation of body growth and strontium levels in the otoliths of the white grunt, *Haemulon plumieri* (Pisces. Haemulidae). *Bull Mar Sci* **50**: 237-257.
[17] Toole CL, RL Nielsen (1992) Effects of microprobe precision on hypotheses related to otolith Sr:Ca ratios. *Fish Bull US* **90**: 421-427.
[18] Philibert J, R Tixier (1968) Electron penetration and the atomic number correction in electron probe microanalysis. *Brit J Appl Phys* **2(1)**: 685-694.
[19] Reed SJB (1993) Electron Microprobe Analysis (2nd Ed.). Cambridge University Press, Cambridge.
[20] Potts PJ (1987) A handbook of silicate rock analysis. Blackie, New York.
[21] Jarosewich E (2002) Smithsonian Microbeam Standards, *J. Res. Natl. Inst. Stand. Technol*. **107**, 681-685.
[22] Jarosewich E, IG MacIntyre (1983) Carbonate reference samples for electron microprobe and scanning electron microscope analyses. *J. Sedimentary Petrol* **52**:677-678.
[23] Jarosewich E, JS White (1987) Strontianite reference samples for electron microprobe and SEM analyses. *J. Sedimentary Petrol* **57**:762-763.
[24] Casting R (1951) Application des sondes electroniques a une method d'analyse ponctuelle chimique et cristallographique. PhD thesis, University of Paris.
[25] Weast RC (editor-in-chief) (1973) Handbook of chemistry and physics (54th edn.). Chemical Rubber Company Press, Cleveland.
[26] Tsukamoto K (1992) Discovery of the spawning area for Japanese eel. *Nature* **356**: 789-791.
[27] Tsukamoto K with 18 coauthors (2011) Oceanic spawning ecology of freshwater eels in the western North Pacific, *Nature Communications* 2, Article number: 179, doi:10.1038/ncomms1174, www.nature.com/ncomms/journal/v2/n2/full/ncomms1174.html
[28] Tzeng WN, JC Shiao, Y Iizuka (2002) Use of otolith Sr : Ca ratios to study the riverine migratory behaviors of Japanese eel *Anguilla japonica. Mar Ecol Prog Ser* **245**:213-221.
[29] Tzeng WN, Y Iizuka, JC Shiao, Y Yamada, H Oka (2003). Identification and growth rates comparison of divergent migratory contingents of Japanese eel (*Anguilla japonica*). *Aquaculture*. **216**:77-86.
[30] Thibault I, JJ Dodson, F Caron, WN Tzeng, Y Iizuka, JC Shiao (2007) Eeels facultative catadromy: a conditional stratery? Facultative catadromy in American eels: testing the conditional strategy hypothesis. *Mar Ecol Prog Ser* **344**:219-229.
[31] Ložys L (2002) Monitoring of glass eel recruitment in Lithuania. In Monitoring of Glass Eel Recruitment (Dekker, W., ed.), pp.87-96. Ijmuiden: Netherlands Institute of Fisheries Research.
[32] Shiao JC, L Ložys, Y Iizuka, WN Tzeng (2006) Migratory patterns and contribution of stocking to the population of European eel in Lithuanian waters as indicated by otolith Sr:Ca ratios. *J Fish Biol*. **69**:749-769.
[33] Lin YJ, L Ložys, JC Shiao, Y Iizuka, WN Tzeng (2007) Growth differences between naturally recruited and stocked European eel *Anguilla anguilla* in Lithuania. *J Fish Biol*, **71**:1773-1787.
[34] Han YS (2012) Wide geographic distribution with little population genetic differentiation: a case study of the Japanese eel *Anguilla japonica*. In Eels: Physiology, Habitat and Conservation (Chapter 7), Eds. S Nakashima and M Fujimoto, pp.149-164. Nova Science Publishers, Hauppauge, USA.
[35] Daverat F, KE Limburg, I Thibault, JC Shiao, JJ Dodson, F Caron, WN Tzeng, Y Iizuka, H Wickström (2006) Phenotypic plasticity of habitat use by three temperate eel species *Anguilla anguilla, A. japonica and A. rostrata. Mar Eco Prog Ser* **308**: 231-241.
[36] Jessop BM, JC Shiao, Y Iizuka, WN Tzeng (2002) Migratory behaviour and habitat use by American eels *Anguilla rostrata* as revealed by otolith microchemistry. *Mar Eco Prog Ser*, **233**:217-229.
[37] Jessop BM, JC Shiao, Y Iizuka, WN Tzeng (2006) Migration of juvenile American eels *Anguilla rostrata* between freshwater and estuary, as revealed by otolith microchemistry. *Mar Eco Prog Ser*, **310**:219-233.
[38] Lamson HM, JC Shiao, Y Iizuka, WN Tzeng, DK Cairns (2006) Movement patterns of American eels (*Anguilla rostrata*) between salt and fresh water in a coastal watershed, based on otolith microchemistry. *Marine Biology*, **149**:1567-1576.
[39] Jessop BM, JC Shiao, Y Iizuka, WN Tzeng (2007) Effects of inter-habitat migration on the evaluation of growth rate and habitat residence of American eels *Anguilla rostrata. Mar Eco Prog Ser*, **342**:255-263.
[40] Jessop BM, JC Shiao, Y Iizuka (2009) Life history of American eels from Western Newfoundland. *Trans Am Fish Soc*, **138**:861-871.
[41] Lamson HM, DK Cairns, JC Shiao, Y Iizuka, WN Tzeng (2009) American eel, *Anguilla rostrata*, growth in fresh and salt water: implications for conservation and aquaculture. *Fishs Manag Ecol*, **16**:306-314.
[42] Tzeng WN, CH Wang, H Wickström, M Reizenstein (2000) Occurrence of the semi-catadromous European eel *Anguilla anguilla* in the Baltic Sea. *Mar Biol*. 137:93-98.
[43] Lin YJ, JC Shiao, L Ložys, M Plikshs, A Minde, Y Iizuka, I Rashal, WN Tzeng (2009) Do otolith annular structures correspond to the first freshwater entry for yellow European eels *Anguilla anguilla* in the Baltic countries? *J Fish Biol*, **75**:2709-2722.
[44] Lin YJ, JC Shiao, M Plikshs, A Minde, Y Iizuka, I Rashal, WN Tzeng (2011) Otolith Sr:Ca Ratios as Natural Mark to Discriminate the Restocked and Naturally Recruited European Eels in Latvia Proceedings of American Fisheries Society Symposium **76**:1-14.